Numerical simulations of long Josephson junctions driven by large external radio-frequency signals

G. Rotoli, G. Costabile, and R. D. Parmentier
Department of Physics, University of Salerno, I-84100 Salerno, Italy
(Received 17 July 1989; revised manuscript received 13 October 1989)

There is experimental evidence in long Josephson junctions of rf-induced dynamical states that are not observed in small junctions. Such states consist of groups of current steps, asymmetrical with respect to the McCumber curve, having amplitudes much larger than the expected rf-induced (Shapiro) steps. Numerical solutions of the model equation (the perturbed sine-Gordon equation) obtained from the multimode expansion are in good agreement (at least qualitatively) with the experimental data. The basic dynamic configuration consists of multifluxon bunches phase locked to the rf signal.

I. INTRODUCTION

Recent experimental work has shown that rf-driven long Josephson junctions (LJJ's), when the external microwave frequency approaches the fundamental geometrical frequency of resonance of the junction, exhibit a number of phenomena that are not observed in small junctions.[1,2] The most evident of such phenomena in the current-voltage (I-V) characteristic can be summarized as follows. First, irradiating the junction with small rf signals, the profile of the zero-field steps (ZFS's) is straightened, producing a constant-voltage current step whose amplitude grows linearly with the power of the driving signal. This phenomenon has been attributed to the phase locking of single-fluxon oscillations (for the first ZFS) to the external signal. It has been investigated theoretically both by solving the perturbed sine-Gordon equation (PSGE) numerically[3,4] and by studying the properties of maps derived from a simplified model of the interaction of a particlelike fluxon with a periodic drive.[5] Secondly, it was observed that irradiating the junction with large rf signals, the usual induced current steps (Shapiro steps[6]) are dominated by current steps, called anomalous current steps (ACS's) in Ref. 7, much larger than what could be expected from existing theories, hysteretic, and strongly asymmetric with respect to the McCumber curve. It was suggested[7] that these steps could be ascribed to the phase locking of multifluxon oscillations to the external rf drive.

To check this hypothesis we have integrated numerically a mathematical model of the LJJ's driven by large rf signals. Our approach uses a multimode expansion,[8] in which the phase is expanded in spatial Fourier components (modes) in order to approximate the PSGE (with its boundary conditions) by a finite set of ordinary differential equations (ODE's). We have solved numerically the ODE system in order to obtain plots of the I-V characteristic and detailed information about the dynamical properties of the phase. We point out that the available literature on the subject of rf-driven LJJ's is concerned mainly with single-fluxon dynamics in the small-rf-field regime, while our main goal is to study the response to large rf fields in order to understand the dynamics of the states corresponding to the ACS's reported from experiments. However, we have also applied our model to the small-field regime to check the consistency of our results with the literature, and also to solve some modeling problems.

The most important of such problems is concerned with the choice of the boundary conditions, i.e., whether it is more realistic to model the interaction of the LJJ's with microwaves by introducing time-dependent boundary conditions representing the rf magnetic field or by adding an rf current term to the PSGE. The former is appropriate to describe a physical situation in which the rf field does not penetrate the junction, so that energy exchange with the rf drive occurs only at the edges, while the latter would correspond to a physical situation in which the energy is exchanged all over the junction. In this work we will follow the first alternative, i.e., we model the rf drive as a boundary magnetic field; we will refer to this approach as the "M model." As a variant of the M model, we have considered a somewhat different model in which the rf drive is introduced as an rf current localized at the junction ends to simulate the effect of weak penetration of the external field into the junction; this approach, which can be useful to deal with a nonuniform field distribution within the multimode approach, will be denoted the "E model" in the following.

We have also carried out numerical calculations following the second alternative, i.e., adding either a spatially uniform or a spatially sinusoidal rf current to the dc-current LJJ bias. As in Ref. 4, we found that with small rf current the phase-locking range is quite small. Increasing the amplitude of the rf current up to several times the critical dc current, we have observed in the I-V characteristic only current steps having small amplitudes, symmetric around the McCumber curve, nonhysteretic, and mixed with chaotic states. Therefore we will not report explicitly these cases.

The solution of the multimode equations allows the reconstruction of the solution of the PSGE with good ap-

proximation and a detailed analysis of the dynamics of the phase in the LJJ's. In particular, we have examined the relation between the phase of the rf drive and the phase of the oscillatory states, and the spatial configuration of the junction phase and its evolution in time to clarify the interior dynamics and its solitonic aspects.

The paper is organized as follows. In Sec. II we give a short description of the multimode approach and describe the numerical techniques adopted to solve the ODE system and to obtain the *I-V* curves. Section III is concerned with the *M* model and the *I-V* characteristics derived from it. Section IV deals with the *E* model and the results obtained from it. In Sec. V we show in some detail examples of the space and time behavior of the phase, reconstructed from the spatial modes, and in Sec. VI we conclude with some remarks about this work and its possible developments.

II. MULTIMODE APPROACH TO THE PSGE

A detailed description of the multimode approach can be found in Ref. 9; here we will consider its extension to the case of time-dependent boundary conditions. Therefore in the following we will outline the procedure that allows one to establish the set of ODE's in the form required by our model. The discussion will be restricted to unidimensional junctions having overlap geometry (i.e., junctions for which the dimension parallel to the dc bias current is much smaller than the Josephson length λ_J).

To introduce the multimode approach we start from the PSGE, which describes the dynamics for the phase in a unidimensional LJJ.[9] In normalized units

$$\phi_{tt}-\phi_{xx}+\sin\phi=\gamma_{\rm dc}-\alpha\phi_t+\beta\phi_{xxt} \ , \tag{1}$$

where $\phi(x,t)$ is the phase difference between the superconductive electrodes, $\gamma_{\rm dc}$ is the constant dc bias current, assumed uniform throughout the junction, α is related to the losses in the tunneling barrier and β to the losses on the electrode surfaces, and subscripts denote partial derivatives. In Eq. (1) lengths are normalized with respect to λ_J, currents are normalized with respect to the junction critical current I_c, and time is normalized with respect to the inverse of the plasma frequency ω_J.

The boundary conditions are assigned by the equations[10]

$$\phi_x(0,t)+\beta\phi_{xt}(0,t)=\phi_x(l,t)+\beta\phi_{xt}(l,t)=\eta(t) \ , \tag{2}$$

where $\eta(t)$ is the magnetic field at the junction ends normalized with respect to $\Phi_0/\mu_0\lambda_J d$, with Φ_0 the flux quantum and d the effective junction barrier thickness (cf. Ref. 9), and l is the normalized junction length.

Next we introduce the multimode expansion of the phase

$$\phi(x,t)=g(t)x+\sum_{m=0}^{N}\theta_m(t)\cos\left[\frac{m\pi x}{l}\right] \ , \tag{3}$$

where the term $g(t)x$ takes into account the boundary conditions with

$$g(t)=\frac{1}{\beta}e^{-t/\beta}\int e^{t'/\beta}\eta(t')dt' \ , \tag{4}$$

and the series is truncated so to provide the required degree of approximation. The choice of the form $g(t)x$ is suggested by consideration of the computational simplicity, as discussed by Costabile *et al.*[11]

Substituting the expansion (3) into Eq. (1) the following set of ODE's is obtained:

$$\ddot{\theta}_0+\alpha\dot{\theta}_0+\frac{1}{l}\int_0^l\sin\phi\,dx=\gamma_{\rm dc}-\frac{l}{2}(\ddot{g}+\alpha\dot{g}) \ , \tag{5a}$$

$$\ddot{\theta}_m+\mu_m\dot{\theta}_m+\omega_m^2\theta_m+\frac{2}{l}\int_0^l\sin\phi\cos\left[\frac{m\pi x}{l}\right]dx=\begin{cases}+\dfrac{4}{\omega_m^2 l}(\ddot{g}+\alpha\dot{g}), & m \text{ odd}\\ 0, & m \text{ even}\end{cases} \tag{5b}$$

where $\omega_m\equiv m\pi/l$, $\mu_m\equiv\alpha+\beta\omega_m^2$, and $m=1,2,\ldots,N$.

With our most frequent choice of the dissipation parameters (i.e., $\alpha=0.025$ or 0.05, $\beta=0.01$ or 0.02), for practical purposes it was sufficient to retain a number of modes equal to twice the normalized length of the junction; the consistency of this assumption was checked in some selected cases by increasing the number of modes. Whenever we set $\beta=0$ (in order to compare our results with the literature) we increased the number of modes to four times the normalized length. In fact, β enters the dissipation parameter multiplied by ω_m^2 [Eq. (5b)], which yields a rapidly growing damping of the higher modes; therefore the elimination of the β term requires more modes to approximate the phase satisfactorily.

For each run $\gamma_{\rm dc}$ was first monotonically increased and then monotonically decreased in the chosen interval to detect the expected hysteretic behavior. To move along the *I-V* curve the bias current was varied in steps of about 0.0005 per unit of time (corresponding to one plasma period) to prevent long transients caused by abrupt changes.

We note that in the multimode approach the average normalized voltage is

$$V_{\rm dc}=\langle\phi_t\rangle_T=\langle\dot{\theta}_0\rangle_T \ , \tag{6}$$

where $\langle\ \rangle_T$ indicates the time average. Equation (6) allows one to plot *I-V* curves by applying simple averaging algorithms to the numerical solution for $\dot{\theta}_0$. We have adopted the most straightforward, calculating $V_{\rm dc}$ from

$$V_{\rm dc}=\frac{\theta_0(t_1)-\theta_0(t_0)}{t_1-t_0} \ , \tag{7}$$

where the time interval t_1-t_0 is to be small with respect to the time interval of the total variation of the bias current, but large with respect to the fundamental period $2\pi/\omega_1=2l$. A good compromise in our case turned out to be from $\sim$30 to $\sim$100 units of time, in order to have an averaging time sufficiently long with respect to the fundamental period and sufficiently short to obtain a number of points to plot the *I-V* curves. With this

choice, the plots that are shown in this paper consist, on the average, of ~60 points. They are readily obtained after the evaluation of V_{dc}, since γ_{dc}, for which we take the value at the midpoint of the interval $t_1 - t_0$, is only a known, time-dependent parameter in our equations. We note that the current steps displayed in our plots of *I-V* characteristics often exhibit small voltage undulations. These undulations are both a consequence of the relatively large integration step size (generally of the order of $T_1/40$, where $T_1 = 2\pi/\omega_1$) of the ODE system, that sometimes can miss a maximum (or a minimum) of the solution and an artifact of the simple averaging procedure used. These undulations might be reduced by using more sophisticated techniques; however, we considered it to be superfluous to reduce the step size of the integration algorithm or to resort to more refined averaging procedures as such procedures would not substantially augment the information already contained in our plots.

To solve the system of Eqs. (5) we used the Bulirsch-Stoer algorithm with adaptive step size.[12] Essentially, at every timestep the integration is performed by building up a series whose terms are the value of the integral obtained dividing the step into progressively smaller substeps; the convergence of the series, evaluated by rational function extrapolation, is assumed to provide the true value. The estimate of the extrapolation error controls the number of substeps needed to obtain the required precision for the actual step size; if this number is larger or smaller than that needed for the last step, the magnitude of the next step size is, respectively, decreased or increased. In this way, relatively large integration step size can be reached without introducing instabilities or divergences. In fact, this algorithm was proved able to integrate the system (5) with step size even larger than $T_1/40$, producing the same results but for the loss of some detail. To evaluate at every step the integrals in Eqs. (5) we used a dedicated discrete-Fourier-transform (DFT) routine that evaluates only the required components. The code was written in FORTRAN and the program run both on a VAX(8200-11/780), with a CPU time of ~10 h and a Cray-XMP48, with a CPU time of ~200 sec for each of the runs needed to build *I-V* curves like those shown in the figures.

III. *M* MODEL

In this section we model the external rf drive by imposing in Eqs. (2)

$$\eta(t) = \eta_0 \sin \Omega t \ , \tag{8}$$

where Ω is chosen close to π/l, the frequency of resonance of the junction. In this way the junction is rf driven by an external magnetic field that acts on the junction only through symmetrical boundary conditions. This assumption reflects the idea of an LJJ immersed in a spatially uniform rf field but not penetrated by the field. Regarding the hypothesis of uniformity, we note that in real experiments the rf wavelength is generally much larger than the physical length of the junction because the velocity of electromagnetic waves in the surrounding medium is always much larger than their maximum velocity in the junction.

It can be proved by direct substitution that Eqs. (2) are satisfied if we assume

$$g(t) = \frac{\eta_0}{(1+\beta^2\Omega^2)^{1/2}} \sin[\Omega t - \arctan(\beta\Omega)] \ . \tag{9}$$

The amplitude and the phase of this expression for the parameter values used differ so slightly from Eq. (8) that, from a practical point of view, one can safely replace $g(t)$ by $\eta(t)$ in the numerical calculations. We emphasize that for a fast convergence of the phase expansion it is convenient to save the simple *ansatz* on the functional form of the g term in Eq. (3); this implies that the method would be unsuitable to describe a configuration relative to a nonsymmetrical distribution of the rf field.

Here we report some of the results obtained with this approach. We have solved numerically the ODE system (5) for values of dissipation parameters commonly adopted in the literature and values of η_0 from 0.2 to 1.0. Figure 1(a) shows the behavior of $\dot{\theta}_0$ as a function of time obtained in the case of $\alpha = 0.025$, $\beta = 0.01$, and $l = 4$; we

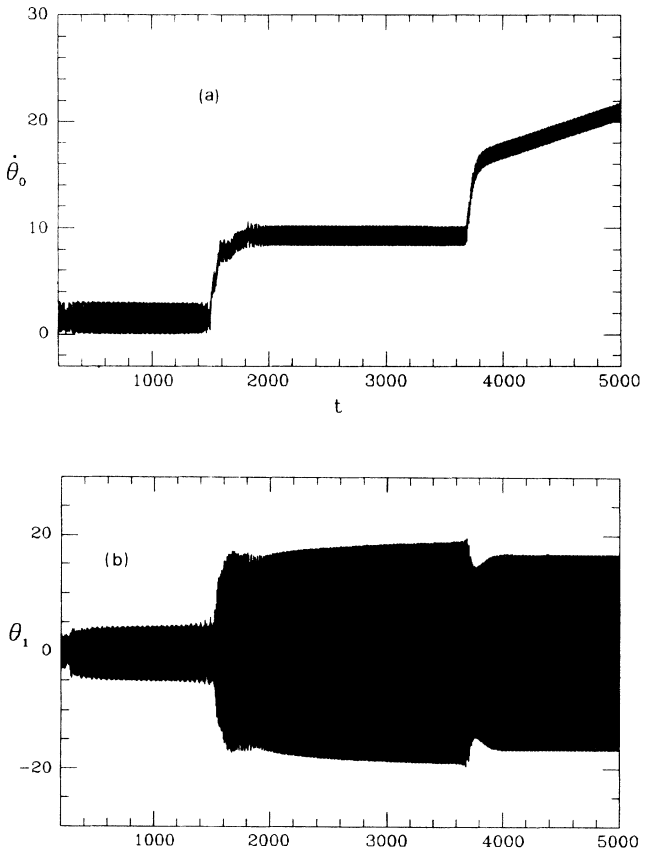

FIG. 1. Solution of Eqs. (5): (a) $\dot{\theta}_0$ and (b) θ_1 as functions of the dc bias, which is increased uniformly in time. Parameters: $\eta_0 = 0.5$, $\alpha = 0.025$, and $\beta = 0.01$. In this and in all the following figures, $l = 4$ and $\Omega = 0.775$.

note that as the dc-bias current is increased uniformly with the time, the average of this oscillation pattern tracks the shape of the I-V curve. The oscillations keep a constant average in the intervals corresponding to the phase-locked states. In Fig. 1(b) we report θ_1, the amplitude of the first mode, for the same time interval; we observe that the amplitude varies as the junction goes from one phase-locked state to the next, while the average is always zero, as expected from the equations. The higher modes show generally the same behavior, but their amplitudes become progressively smaller as m is increased. We point out that the information in Figs. 1(a) and 1(b) is provided by the envelope of the pattern; the different density of the grey shade has no physical significance, being nothing more than a numerical artifact caused by both the variation of the time-step size and the amplitude of the time interval chosen to sample the data.

Inasmuch as little theoretical or numerical information concerning the large rf-drive regime exists in the literature, we prefer to start from the analysis of the small-drive regime, in order to compare our results with those obtained by other authors. The most straightforward test is to calculate the modification induced on the I-V characteristic of the first zero-field step (ZFS1) in this limit. A typical result is reported in Fig. 2. We see clearly a straightening (the full curve) of the unperturbed ZFS1 (the dotted curve) where single-fluxon oscillations are phase locked to the external signal. For phase locking at the fundamental frequency, the voltage of the rf-induced step is given by $V=2\Omega$, where Ω is the drive frequency. Accordingly, the step in Fig. 2 appears at $V=1.55$. For comparison, the asymptotic limiting voltage for the unperturbed ZFS1 is given by $V_a=2\pi/l$, which for Fig. 2, gives $V_a=\pi/2$. A simple analysis says that the height in current of the step should be $\Delta\gamma_{dc}=4\eta_0/l$; the step height in Fig. 2 is consistent with this estimate. A noteworthy feature of Fig. 2 is the existence of frequency pulling outside of the phase-locking region, i.e., for bias current below the rf-induced step the profile of the ZFS is pulled to higher voltages. This phenomenon seems to be enhanced by the presence of a nonzero β-loss term.

An independent way to identify the phase-locked states is to analyze the relation between the spatial configuration of our numerical solutions with the phase of the external fields. To this end we have plotted the voltage of one junction end versus the phase of the rf field. Inspection of this kind of plot signals the phase locking by the fact that the junction-end voltage peak caused by reflection of fluxons takes and maintains a constant phase difference with respect to the external signal. Figure 3 refers to the phase-locking zone on ZFS1 as

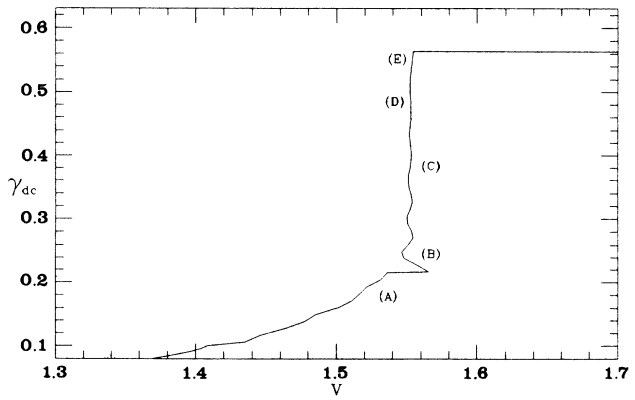

FIG. 2. Phase locking on ZFS1 with the M model. The dotted line is the I-V characteristic when no rf field is applied. Parameters: $\eta_0=0.2$, $\alpha=0.025$, and $\beta=0.01$.

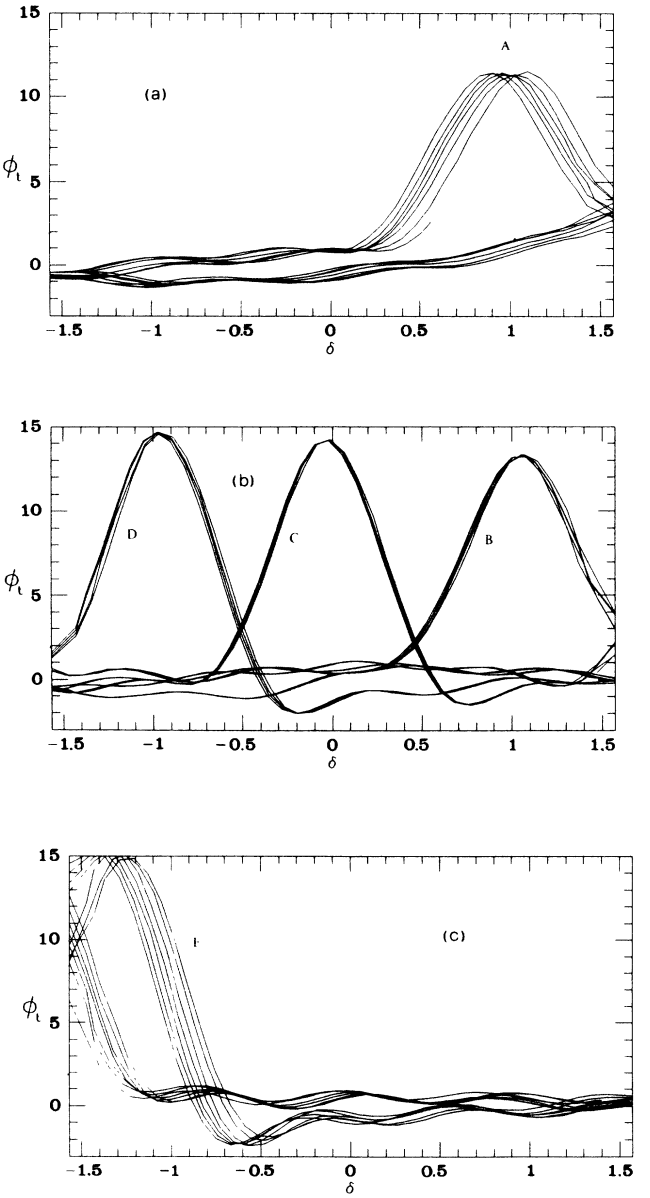

FIG. 3. Voltage at one end of the junction vs the phase (δ) of the rf drive when the junction is biased on the points indicated by capital letters in Fig. 2. The family of curves in each state is obtained tracking the voltage continuously in time.

shown in Fig. 2. Figure 3(a) shows the reflection peak through successive reflections at the end of the junction in the point marked (A) in Fig. 2, i.e., in a current region below the phase-locking region. The peak is shifted after each period; from this we infer that the phase delay is not constant and that we do not have phase locking. Figure 3(b) shows the reflection peaks at three successive points in the phase-locking region marked by (B), (C), and (D) in Fig. 2. We see that in these cases the phase delay is constant, i.e., the peak overlaps itself after each period. We note that the reflections are approximately coincident with the maximum of the rf signal at the bottom (positive maximum) and at the top (negative maximum) of the step, and near the zero of the rf signal in the middle of the step, in qualitative agreement with the results reported in Refs. 4 and 5. Figure 3(c) shows the reflection peak at the point (E) in Fig. 2, where we have a situation similar to that of Fig. 3(a): the peak is shifted and we do not have phase locking. As noted by Davidson and Pedersen,[4] this analysis is equivalent to some extent to a Poincaré map; it therefore allows the identification of states that can be strictly defined phase-locked states, whereas the information provided by Fig. 2 should be considered as indicative of frequency-locked states because it is relative to time averages over several periods.

The position of the reflection peak with respect to the phase of the rf-signal is indicative of the amount of energy that the external field has to supply to the junction to keep the fluxons in the phase-locked state. In fact when the frequency of the rf signal is closer to the frequency of the free oscillation [cf. Fig. 3(b), points (C) and (D)] the phase is closer to zero, while it grows [Fig. 3(b), point (B)] when the frequency of the free state is further off. Figure 3(a) shows that the rf field in that case cannot phase lock the fluxon, not even by transferring the maximum amount of energy available.

As a further test we have set $\beta=0$ in order to check the consistency of our approach with the results obtained by other procedures. We show in Fig. 4 a run with $\alpha=0.025$ and $\beta=0$ to make a qualitative comparison with map simulations of the type reported by Salerno *et al.*[5] Figure 4 shows, with the remaining parameters

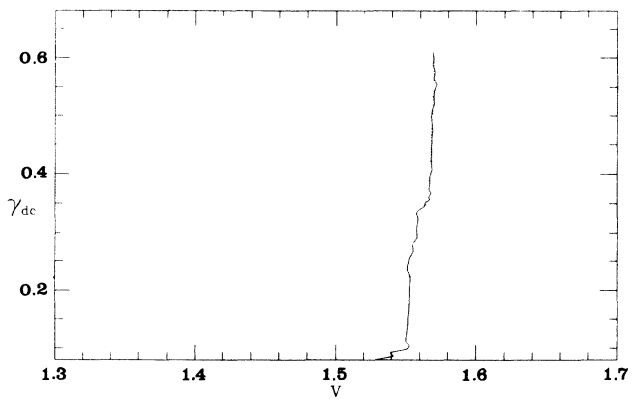

FIG. 4. Plot of ZFS1. The parameters are the same as in Fig. 2, but for $\beta=0$.

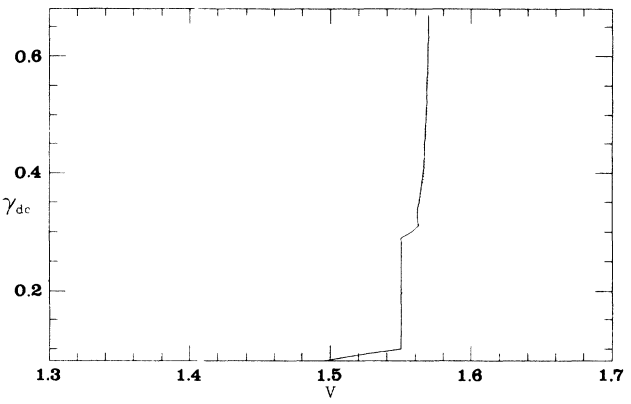

FIG. 5. Same as in Fig. 4, reported from map simulation.

equal to those used in Fig. 2, the I-V characteristics of ZFS1 calculated using the multimode equations, to be compared with Fig. 5, which shows the results obtained for the same parameters with the map approach. We note that the shape of ZFS1 and the height of field-induced straightening is very similar in both cases.

We think that the instability observed in the upper part of the current step in Fig. 4 is related to the vanishing of the β-term: the stability is decreased because the dissipation affecting the spatial modes is reduced. The obvious remedy would be to increase the number of modes used, at the price of an increased CPU time, but this would render inconvenient the multimode approach: as indicated earlier, this approach is convenient when the series in Eq. (3) converges rapidly, which requires that β be not too small. This fact does not constitute a real drawback inasmuch as real junctions always exhibit non-negligible surface losses. If we restore the β term in our equations, the instability disappears and the characteristic returns to that shown in Fig. 2.

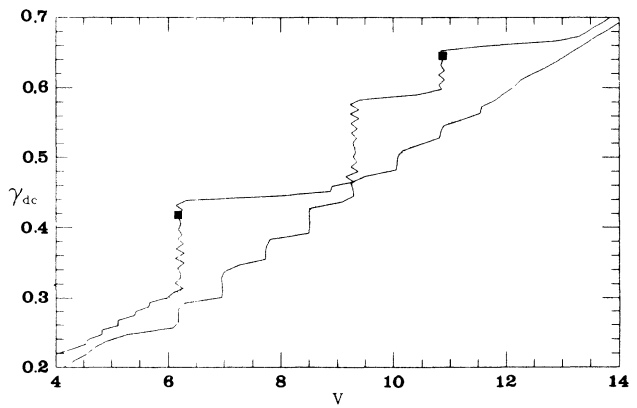

FIG. 6. I-V characteristic calculated from the M model with $\eta_0=0.7$, $\alpha=0.05$, and $\beta=0.02$. The upper (lower) curve is obtained by increasing (decreasing) the dc bias monotonically. The dotted line is the I-V characteristic of the undriven junction.

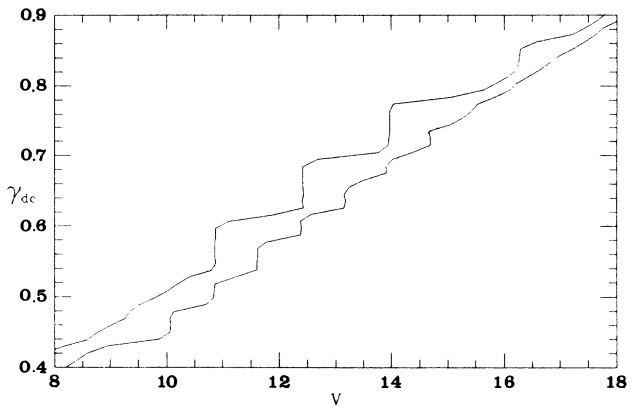

FIG. 7. Same as Fig. 6, but for $\eta_0=1.0$.

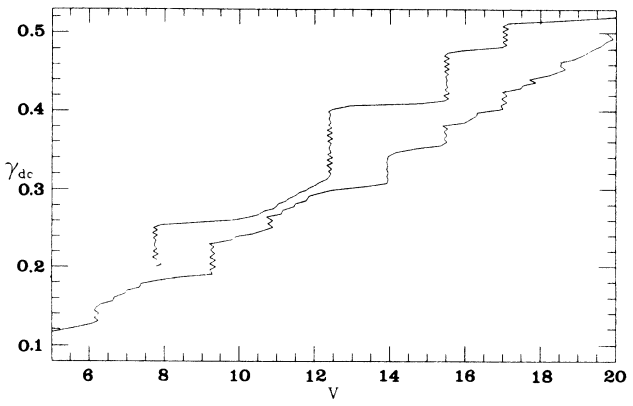

FIG. 9. *I-V* characteristic as in Fig. 6, but for $\beta=0.01$.

Now we analyze the case of large rf-drive signals. The distinction between the two types of regimes will be more clear when we analyze the internal dynamics of the junction; however, in general we speak of *large signal* when we observe rf-induced current steps in the *I-V* characteristic at voltages higher than that of ZFS1. In Fig. 6 we show a typical result obtained in the large-signal simulations: the junction exhibits current steps up to a normalized voltage of 14Ω, as compared with $V=2\Omega$ for ZFS1. We note that the upper branch of the steps, obtained by integrating Eqs. (5) with increasing current bias, is detached from the lower branch, obtained by decreasing the current bias. However, this is only a computational artifact, attributable to the fact that the current bias has been varied monotonically; in fact, starting from the lower branch and increasing the dc current, it is always possible to track the whole step with continuity. In Fig. 7 we show the result with a larger value of η_0, which moves the leading steps to higher voltages; this behavior should be compared with the experimental results reported by Monaco *et al.*,[7] reproduced in Fig. 8. The plot of Fig. 9 has been made with the same parameters of Fig. 6, but with lower dissipation. We observe that the behavior is qualitatively the same; the phase-locked states are again only shifted higher on the *I-V* curve.

All of our plots show some common features: (a) the steps are asymmetric with respect to the McCumber curve; (b) even-order steps are much larger than odd-order steps; (c) the step staircase moves higher on the McCumber curve when η_0 is increased; and (d) the staircase is hysteretic. We remark that all these common features are observed in the actual experiment as can be seen in Fig. 8.

The last question is what happens in the large-signal regime to the phase relation with the external field? To answer this question we have analyzed a number of cases, from which we show in some detail the one relative to the *I-V* characteristic of Fig. 10. Thus, we have in Fig. 11(a) the reflection peak corresponding to the point marked (*A*) in Fig. 10; again we observe that we have an unlocked situation. Figure 11(b) represents the situation corresponding to the three points (*B*), (*C*), and (*D*) in

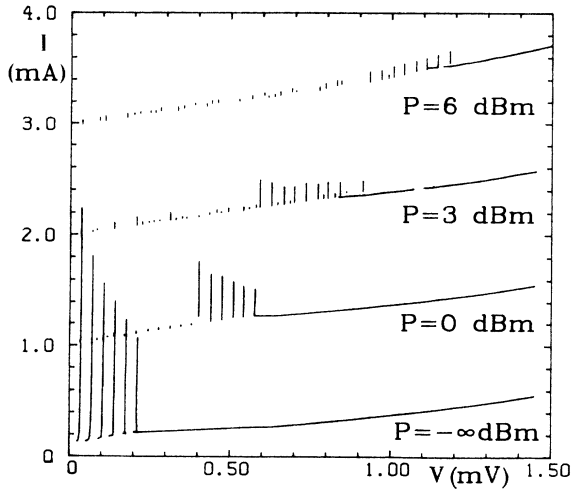

FIG. 8. Experimental plot of ACS's from Monaco *et al.* (Ref. 7).

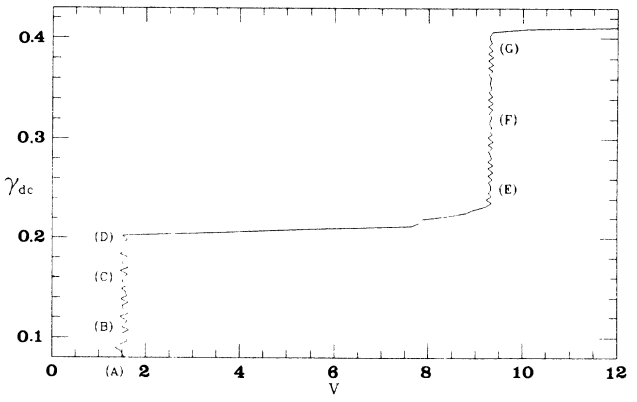

FIG. 10. *I-V* characteristic obtained using the *M* model. Parameters: $\eta_0=0.5$, $\alpha=0.025$, and $\beta=0.01$.

Fig. 10. Since the lower step is at $V=2\Omega$, the phase relation can be compared with that of Figs. 2 and 3. The main difference with respect to locking on ZFS1 is exemplified by comparing the behavior for $\gamma_{dc}\sim 0.2$ [point (D) in Fig. 10 and point (B) in Fig. 2]: the phase of the external signal is reduced by a factor of about 2. This can be again interpreted in terms of the energy that must be provided by the rf signal to lock the fluxon: when η_0 is larger, the phase must adjust itself to a lower value to transfer the same amount of energy. At the bottom of the step, point (B), where the bias current in the free state would correspond to a voltage much lower than the step voltage, the reflection again occurs near the rf maximum because more energy is required to phase lock the fluxon. Figure 11(c) shows the situation relative to the successive phase-locked states corresponding to points (E), (F), and (G) in Fig. 10. The same behavior seen in Fig. 11(b) is approximately repeated here; the spread of the voltage peak is caused by the presence of more fluxons, as we will demonstrate in Sec. V.

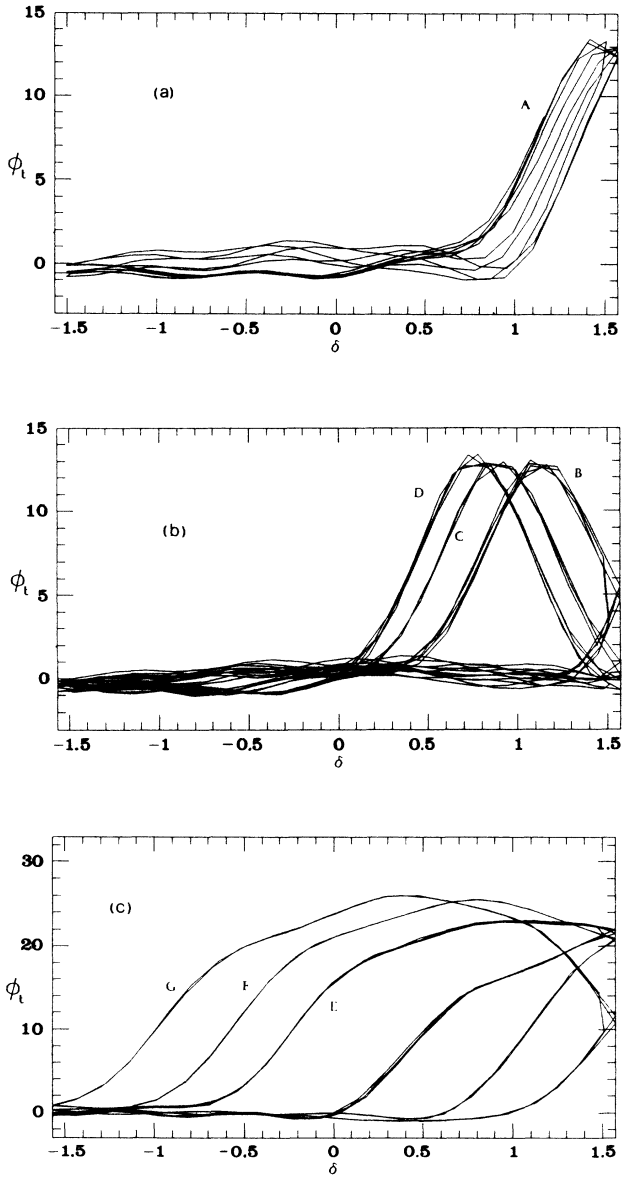

FIG. 11. Voltage at one end of the junction as a function of the phase (δ) of the rf drive when the junction is biased at the points indicated by capital letters in Fig. 10. Note that point (A) is slightly shifted toward the left of the step.

IV. E MODEL

On the basis of physical intuition, the effect on an LJJ of the rf signal modeled by the boundary conditions (2) can be thought equivalent to the application of suitable currents at the junction edges. In the case of a static or quasistatic magnetic field, one can calculate an appropriate current profile by following the analysis of Owen and Scalapino.[13] In the high-frequency limit there is some degree of uncertainty in the choice for the shape of the function that has to model the rf field. One can reasonably guess that any function decaying in the junction over a typical length of the order of λ_J could serve to model the rf current at the edges, causing phase-lock effects not far from those obtained with the M model. Therefore, we have made the following choice: the boundary conditions are simplified to the trivial form

$$\phi_x(0,t)+\beta\phi_{xt}(0,t)=\phi_x(l,t)+\beta\phi_{xt}(l,t)=0\ , \tag{10}$$

while a current term having the form

$$\gamma_{ac}(x,t)=\gamma_0(e^{-x/w}-e^{-(l-x)/w})\sin\Omega t \tag{11}$$

is added to the right-hand side of Eq. (1). As a consequence, in Eqs. (5) the Fourier coefficients of $g(t)x$ must be replaced by the Fourier coefficients of $\gamma_{ac}(x,t)$. Equation (11) contains two parameters: w, the penetration depth, and γ_0, the normalized current amplitude. While w can be safely assumed comparable to λ_J, γ_0 is essentially arbitrary; in practice, it has been taken as an adjustable parameter.

We have performed numerical calculations both with symmetric and asymmetric rf drives [the latter was simulated simply by eliminating one of the exponential terms in Eq. (11)]. We will not report plots relative to these calculations, as they do not add qualitatively new information. In fact, using the same parameters that had been adopted for the M model, we obtained I-V characteristics that showed essentially the same features of those reported in Figs. 4, 6, 7, and 9: asymmetric steps, mostly at even-order voltages, moving higher on the characteristic as the amplitude of the rf drive is increased.

We stress that the whole procedure in our treatment of the E model is clearly *ad hoc* and, we emphasize, is based mostly on physical intuition; nevertheless, we think it is worth pursuing because its good qualitative agreement with the results of the M model provides a convenient tool to manipulate rf fields that are spatially nonuniform. In particular, it can prove useful to study the system comprised of two junctions coupled to each other by the radiation received and emitted at one of the edges, which evidently involves an asymmetric drive.

V. ANALYSIS OF THE PSGE SOLUTION

As already mentioned, the approximate solution $\phi(x,t)$ to the PSGE must be reconstructed by summing up all modes in Eq. (3). A series of plots representing the phase along the junction is shown in Fig. 12; they are relative to the phase-locked state marked with a filled square on the 14th step of Fig. 6. The plots are pictures of ϕ taken at successive times, separated by intervals of about $T_1/40$; therefore the entire figure spans a complete period. We see that the maximum elongation (difference of phase between the two ends of the junction) measured from the figure after a semiperiod [curve (A)] is approximately $\Delta\phi_{\rm num}\sim 36.7$ (where with $\Delta\phi_{\rm num}$ we indicate the elongation measured directly from the numerical data), which is close to 12π; hence, the spatial configuration of the phase at that instant can be visualized as consisting of a bunch of approximately six kinks. From this state the situation evolves toward a progressive annihilation of the bunch because of the reflection occurring at the left end of the junction; the half-point of the reflection is characterized by a minimum in the elongation, which drops to ~ 0 [curve (B)]. Then the bunch of kinks emerges again and propagates toward the right end [curve (C)], until the process is repeated [curve (D)] with a reflection at the right end. Therefore, at a first glance the dynamics appears to involve multifluxon (MF) oscillations. For such objects we can give a precise relation between the number of fluxons involved and the voltage.

With reference to Fig. 6, if the voltage of the marked state should be ascribed only to MF oscillations, then there should be a bunch of seven kinks in the junction: in fact we obtain

$$V=\langle\phi_t\rangle=\Delta\phi_{\rm th}/T=2n_{\rm kinks}2\pi(\Omega/2\pi)=14\Omega\ .$$

The corresponding elongation of the phase, for a semiperiod, would be $\Delta\phi_{\rm th}=(\frac{1}{2})28\pi\sim 43.9$. But the maximum elongation in Fig. 12 is never that large and, hence, cannot account alone for the average voltage. The discrepancy can be resolved by taking into account the spatially uniform rotation of the phase, which contributes significantly to the total voltage. The picture that emerges from these considerations is one of kink oscillations superimposed upon an overall rotation of the phase. We found that this result is quite typical: in the states belonging to the current steps the phase is "twisted" so as to originate a bunch of kinks in oscillatory motion; however, though we found that the number of kinks becomes larger as the current is increased toward the top of the step, in general for high-order steps it turns out to be smaller than what would correspond to the step voltage. Therefore one can argue that the phase along the junction must undergo an overall rotation that adds to the kink oscillations and offsets the $\langle\phi_t\rangle_T$ up to the proper value. As we have found in the cases we examined that this argument holds true, we suggest that the dynamics of the phase can be considered in general as consisting of the periodic oscillation of bunched kinks "surfing" over a rotating background.

We have found that there are also states consisting of pure MF dynamics; they are mostly located in the lower part of the I-V characteristic. An example, relative to the state corresponding to the point marked in Fig. 6 on the eighth step (whose voltage is four times larger than that of ZFS1), is shown in Fig. 13. The series of plots appears qualitatively very similar to the one of Fig. 12, and again we observe the same MF dynamics; however, here the MF oscillation can account by itself for the voltage of the eighth step. In fact, the maximum elongation in this case is $\Delta\phi_{\rm num}\sim 27.2$ and is roughly equal to $\frac{1}{2}16\pi$, which is the elongation required to reproduce the step voltage.

For large signals we can relate the observed number of kinks in the junction to the value of the external field η_0 by the following simple argument. Considering that the number of kinks when the elongation takes its maximum value is essentially dominated by the amplitude of the first mode, which is much larger than the higher-order modes, we can write with good approximation $\Delta\phi\sim 2\theta_1$.

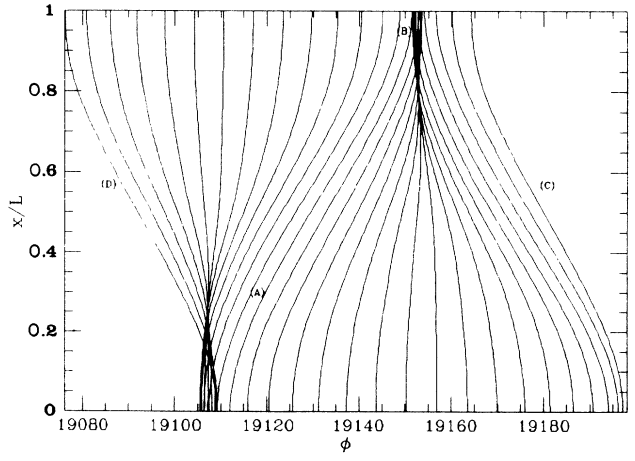

FIG. 12. The phase ϕ along the junction at equally spaced time intervals during a period of the rf signal. The state is indicated by the square dot on the highest step in Fig. 6.

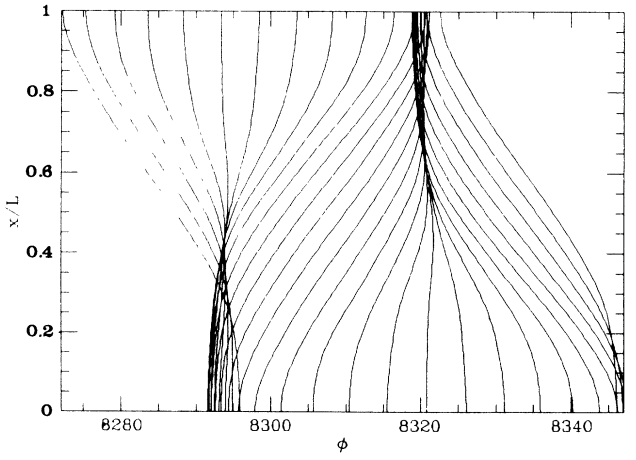

FIG. 13. Same as Fig. 12 for the state identified by the filled square on the lowest step in Fig. 6.

On the other hand, we know that the amplitude of the first mode is the solution of the first equation of the ODE system [Eq. (5b)]. Looking at the system we can observe that strong fields will tend to linearize the equations for the spatial modes, since the Fourier coefficients grow linearly with the field via η_0, while the magnitude of the parametric terms (the integrals) is limited by the $\sin\phi$ term. On this basis we can linearize the first mode equation by dropping the parametric term, obtaining in this way a simple oscillatory equation whose solution will be a linear function of η_0. The validity of this approximation can be checked from Fig. 14, where we compare the maximum and minimum values of the peak-to-peak amplitude of the first mode (for the values of η_0 used in our numerical simulations) with the linear approximation: the difference between the maximum and minimum is less than 2π when $\eta_0 > 0.7$, which means that evaluating the number of kinks with the linear approximation for these values of η_0 we have substantially the correct prediction. We note that the shrinking of the variation of the first mode for growing η_0 implies that the number of fluxons that determines an I-V characteristic for large rf signals is almost constant; the order of the steps is determined mostly by the uniform rotation.

If we plot the voltage range in which the steps occur as a function of η_0 and compare it with the average number of kinks provided by the linear approximation, we can get some useful indication of the relative weight of the two mechanisms, MF and rotation, that are responsible for the total voltage. First, we have to rescale the elongation in units of the characteristic voltage $\tilde{V} \sim \Delta\phi/\Omega$; using the linear approximation we obtain $\tilde{V} \sim 2\rho\eta_0/\Omega$, where

$$\rho = [(\omega_1^2 - \Omega^2)^2 + \mu_1^2\Omega^2]^{-1/2}$$

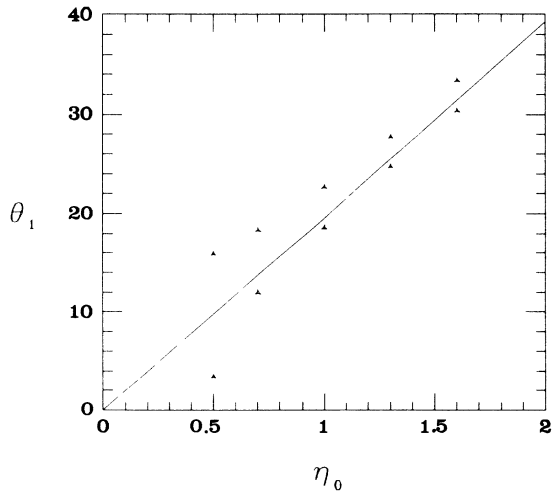

FIG. 14. Maximum and minimum of peak-to-peak amplitude of θ_1 for some values of the amplitude of the rf field. The solid line is the linear approximation. Parameters: $\alpha = 0.05$ and $\beta = 0.02$.

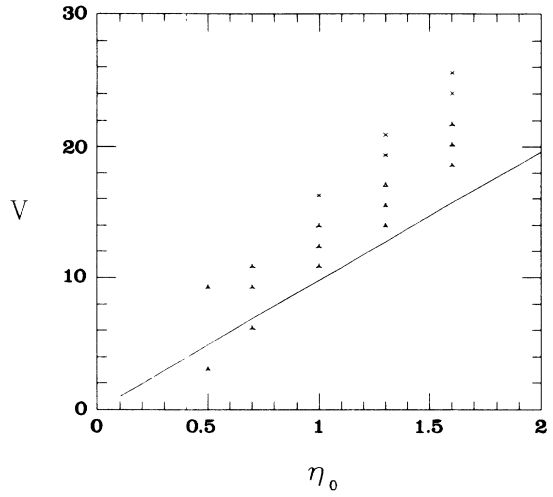

FIG. 15. Voltage of the steps whose amplitude differs significantly from zero, plotted as in the last figure, using the same parameters. The solid line is the linear approximation. Even-order steps are marked by triangles, and odd-order steps by crosses.

is the resonance amplitude for the linearized first mode equation. This voltage yields the position at which steps on the I-V characteristic are not affected by any additional rotation; in fact, for a step at this value of voltage we have

$$V \sim \tilde{V} \Longrightarrow \Delta\phi_{\text{th}}/\Omega \sim 2\rho\eta_0/\Omega \sim \Delta\phi_{\text{num}}/\Omega \ . \tag{12}$$

In Fig. 15 we show for five values of η_0 the voltage range covered by the most significant steps on the I-V characteristic (for the sake of completeness we also include the case $\eta_0 = 0.5$, for which the linear approximation is, indeed, quite poor). We note that the leading steps start approximately at $\tilde{V}$, and therefore the first step is generally a pure MF step, while higher-order steps show a growing content of rotation. Also, the dc-bias current and the ac external field play different roles: in the higher region of the I-V characteristics the rotation is determined by the dc bias, while the number of kinks is determined by the amplitude of external field.

We show in Fig. 16 some plots of ϕ_t (instantaneous voltage) and ϕ_x (instantaneous longitudinal current) in the junction for a cycle of the rf. The shape of the current distribution looks similar to that of a linear cavity at resonance, except in the reflection zones, where distinct curvature appears because of the packing of fluxons entering or emerging from the edge in the bunch. This observation is helpful to better understand to which extent the linear approximation can be assumed to hold.

Finally, we remark that the transition between steps is a quite abrupt phenomenon that lasts about one plasma period; such a switching time is orders of magnitude faster than the transients that we usually observed in our simulations.

VI. CONCLUSIONS

The numerical simulations carried out in this paper show that with a simple hypothesis on the interaction of the junction with the external fields the multimode approach can describe the dynamics of phase-locked states that, in the case of small rf signals, are coincident with those investigated by other theoretical models, and, for larger rf signals, exhibit the essential features of the states observed in actual experiments. Moreover, the mode

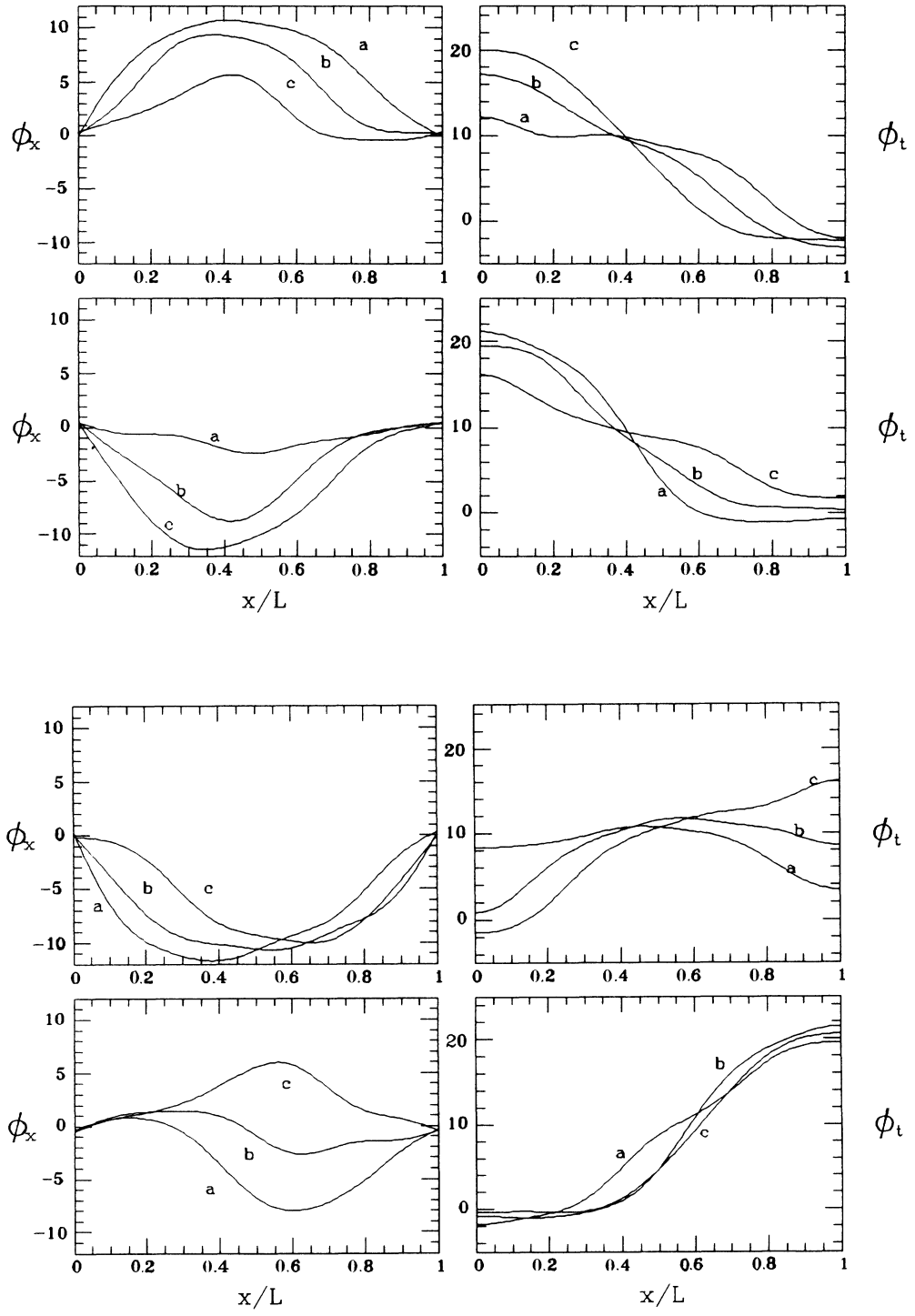

FIG. 16. Series of plots of ϕ_t and ϕ_x along the junction at successive times, equally spaced, during a period of the rf signal.

analysis provides a quite intuitive picture of the dynamics for large rf field, since it helps to clarify to which extent the solitonic aspect is important for the generation of the current steps in the I-V characteristic. The progressive linearization of the problem is made evident in Fig. 14, and can be taken as a starting point to develop an approximate analysis for large rf fields that can be useful for the purpose of applications. As an example, let us consider Eq. (5a) in the linear approximation, i.e., when the integral representing the parametric interaction with the higher modes is negligible with respect to the external drive (both dc and rf); in the I-V characteristic this would correspond to a high-order current step. Dropping the integral, Eq. (5a) turns into the equation for a linear, driven and damped rotator which, we remark, cannot be phase locked inasmuch as the right member only adds energy to the system, rather than adding or subtracting according to the value of the bias current, as is required for phase locking. In other words, neglecting the term $\alpha\dot{g}$ since it is much smaller than $\ddot{g}$, the inequality

$$\gamma_{\rm dc}-\frac{l}{2}\ddot{g}\geq 0 \tag{13}$$

gives an upper bound to the maximum current at which phase-locked states can occur. With trivial calculations, taking into account that near the resonance $\Omega\sim\pi/l$, one gets

$$(\gamma_{\rm dc})_{\rm max}=\frac{\eta_0\pi^2}{2l}\ . \tag{14}$$

The linear approximation then allows us to write Eq. (14) explicitly in terms of voltage

$$V_{\rm max}=\frac{\eta_0\pi^2}{2\alpha l}\ , \tag{15}$$

in order to make a comparison with the results obtained integrating Eqs. (5). Taking for this comparison the data of Fig. 15, we find that for the three largest values of η_0, in growing order, the maximum step voltage is, respectively, 67%, 71%, and 74% of the upper bound predicted by Eq. (15). This fact is consistent with the hypothesis that the higher we move on the I-V characteristic, the more the linear approximation is justified. The upper bound for the step voltage can be an important condition for devices using rf-driven LJJ's, but there are also two other consequences of Eq. (15) that are worth pointing out. The first is that for a fixed value of the voltage (i.e., of the step order), η_0 is directly proportional to l: the longer the junction, the larger the rf drive must be to phase lock the junction on the highest step. The second is that near the resonance the frequency does not play any role: the height of the staircase is virtually frequency independent.

We aim to extend this study to the mutual coupling of Long Josephson junctions and their phase locking to external rf fields in order to obtain information that could be interesting both for nonlinear dynamics and for applications.[7]

ACKNOWLEDGMENTS

We are pleased to acknowledge fruitful discussions with R. Monaco and S. Pagano. We are grateful for the financial support received from the European Economic Community through Contract No. St-2-0267-J-C(A), from the Ministero della Pubblica Istruzione (Italy), and from the Cray Project of the Consiglio Nazionale della Ricerche (Italy).

[1]G. Costabile, R. Monaco, and S. Pagano, J. Appl. Phys. **63**, 5406 (1988).
[2]G. Costabile, V. P. Koshelets, R. Monaco, and S. Pagano, Jpn. J. Appl. Phys. **26**, 1639 (1987).
[3]M. Cirillo, J. Appl. Phys. **60**, 338 (1986).
[4]A. Davidson and N. F. Pedersen, Appl. Phys. Lett. **55**, 1132 (1989).
[5]M. Salerno, M. R. Samuelsen, G. Filatrella, S. Pagano, and R. D. Parmentier, Phys. Lett. A **137**, 75 (1989).
[6]S. Shapiro, Phys. Rev. Lett. **11**, 80 (1963).
[7]R. Monaco, S. Pagano, and G. Costabile, Phys. Lett. A **124**, 523 (1987).
[8]S. Pagano, M. P. Soerensen, R. D. Parmentier, P. L. Christiansen, O. Skovgaard, J. Mygind, N. F. Pedersen, and M. R. Samuelsen, Phys. Rev. B **33**, 174 (1986).
[9]S. Pagano, Ph.D. thesis, Technical University of Denmark, 1987.
[10]J. C. Eilbeck, P. S. Lomdahl, O. H. Olsen, and M. R. Samuelsen, J. Appl. Phys. **57**, 861 (1985).
[11]G. Costabile, S. Pagano, and R. D. Parmentier, Phys. Rev. B **36**, 5225 (1987).
[12]W. H. Press, B. P. Flannery, S. A. Teukolsky, and W. T. Vetterling, *Numerical Recipes* (Cambridge University Press, Cambridge, 1986), Chap. 15.
[13]C. S. Owen and D. J. Scalapino, Phys. Rev. **164**, 538 (1967).